

ISSN No. 2454-6194 | DOI: 10.51584/IJRIAS | Volume X Issue X October2025

# Effects of Thermal Radiation and Ohmic Heating on hydromagnetic Maxwell Hybrid Nanofluid Flow

Francis Kirwa Korir (B.Sc.)

Department of Mathematics and Actuarial Science, Kenya

DOI: https://dx.doi.org/10.51584/IJRIAS.2025.10100000183

Received: 28 October 2025; Accepted: 04 November 2025; Published: 22 November 2025

## **ABSTRACT**

The constitutive model for the Maxwell fluid is mostly used in the polymeric industry to model the flow of viscoelastic fluids. Since 2005, fluids properties have been enhanced by the emergence of nanofluids and hybrid nanofluids. Studies on Maxwell hybrid nanofluid have been carried out under different conditions, but the effects of both thermal radiation and ohmic heating on the hydromagnetic Maxwell hybrid nanofluid flow has not been investigated. Motivated by this, this study probes into the role that thermal radiation and ohmic heating plays on a 2-D incompressible hydromagnetic flow of Maxwell hybrid nanofluid; a suspension of both Alumina/Copper nanoparticles in a Maxwell fluid. The model of the is formulated then transformed into a non-dimensional system using similarity variables. The shooting technique is employed to convert the dimensionless equations to their equivalent initial value problem; which is then solved using MATLAB bvp4c solver. Parametric analysis shows: Grashof number  $(1\rightarrow7)$  increases velocity 35%, decreases temperature 28%; magnetic parameter  $(1\rightarrow7)$  raises temperature 60%, reduces velocity 71%; nanoparticle fraction  $(1\%\rightarrow4\%)$  elevates temperature 22%, lowers velocity 18%; radiation parameter enhances heat transfer 31%; Weissenberg number reduces boundary layer 42%.

#### INTRODUCTION

## **Background of the study**

Fluids are classified into Newtonian and non-Newtonian categories based on their viscosity behavior under shear stress. Maxwell fluid, a viscoelastic non-Newtonian model proposed by James Clerk Maxwell in 1867, finds extensive applications in polymeric industries for manufacturing coatings, hydrogels, batteries, and drug delivery systems. Understanding Maxwell fluid behavior is crucial for optimizing polymerization processes in terms of energy efficiency and cost reduction.

To enhance the thermal and electrical properties of conventional fluids, nanotechnology introduced the concept of adding nanoparticles (1-100 nm) to base fluids. Hybrid nanofluids, formed by dispersing two different nanoparticle types, demonstrate superior thermophysical properties compared to mono-nanofluids and conventional fluids (Ahmed et al., 2024; Raghu et al., 2024). These enhanced fluids are applied in transformers, electronics cooling systems, biomedical applications, and polymeric industries due to their exceptional thermal conductivity, electrical conductivity, and mass transfer performance.

This study focuses on Al<sub>2</sub>O<sub>3</sub>-Cu/water Maxwell hybrid nanofluid, a combination recognized for its thermal stability, excellent conductivity, and corrosion resistance (Zainal et al., 2022; Jaafar et al., 2022). Recent investigations have demonstrated that Cu-Al<sub>2</sub>O<sub>3</sub> hybrid nanofluids exhibit 12-20% enhanced heat transfer rates compared to mono-nanofluids (Shamshuddin et al., 2023), making them ideal candidates for advanced thermal management applications.

When an electrically conducting fluid flows through a magnetic field, the resulting hydromagnetic (MHD) behavior significantly influences flow characteristics and heat transfer mechanisms. Govindarajulu and Subramanyam Reddy (2022) investigated MHD pulsatile flow of third-grade hybrid nanofluids, demonstrating that magnetic field intensity critically affects temperature distribution and velocity profiles. This study examines two-dimensional, incompressible MHD flow of Maxwell hybrid nanofluid over a linearly moving





surface, incorporating the combined effects of thermal radiation and Ohmic heating—two phenomena rarely analyzed simultaneously in Maxwell hybrid nanofluid systems.

Thermal radiation, governed by the Stefan-Boltzmann law, plays a critical role in high-temperature environments where conventional heat transfer modes become less effective. In fluid mechanics applications such as aerospace thermal shields, nuclear reactors, and industrial heat exchangers, radiative heat transfer significantly impacts system performance (Jayaprakash et al., 2024). Algehyne et al. (2024) demonstrated that thermal radiation enhances temperature distribution in Casson hybrid nanofluids by up to 18% under MHD conditions with Ohmic heating effects.

Ohmic heating, arising from electrical resistance in conducting fluids subjected to magnetic fields, generates internal heat that influences thermal behavior. Samuel and Olajuwon (2022) analyzed Ohmic heating effects in chemically reactive Maxwell fluids, revealing that the Brinkman number significantly affects temperature profiles and heat transfer rates. Recent studies by Ahmed et al. (2024) on non-linear radiative Maxwell nanofluids further confirm that Ohmic heating combined with thermal radiation creates synergistic effects that enhance thermal performance in industrial applications.

The novelty of this research lies in investigating the simultaneous effects of thermal radiation and Ohmic heating on Maxwell hybrid nanofluid (Al<sub>2</sub>O<sub>3</sub>-Cu/water) flow in an MHD environment—a combination with significant implications for advanced thermal management in manufacturing processes, energy systems, and materials processing industries. By examining these coupled phenomena, this study aims to provide insights for optimizing heat transfer in industrial applications requiring precise thermal control under electromagnetic conditions.

#### **Statement of the Problem**

Investigation into the role of thermal radiation on the flow of hybrid Maxwell nanofluid over rotating surfaces, as well as shrinking and stretching surfaces, has garnered significant attention in recent research. However, there has been limited focus on understanding the impact of ohmic heating over a surface that linearly stretches in a magnetic hybrid Maxwell nanofluid context. To address this gap, the proposed work aims to explore the influence of thermal radiation and ohmic heating on hydromagnetic Maxwell hybrid nanofluid flow. The base fluid is the molten polyethylene, with alumina and copper nanoparticles chosen as nanoparticles. This study seeks to provide a clearer understanding of the interactions between heat transfer, fluid flow, and magnetic fields in such systems, offering insights valuable for various industrial applications and theoretical advancements in fluid dynamics.

## **Justification of the Study**

Maxwell fluid is a very useful viscoelastic model in the polymeric industry. On its own, its conductivity is poor but when nanoparticles are added, the conductivity and other fluid properties are enhanced significantly. The use of alumina-copper nanoparticle combination has proven to be very effective in the hybridization process due to its stability, magnificent conductivities and resistance to corrosion. As a result, this study uses Maxwell as a base fluid and alumina-copper combination as the nanoparticles. Quite a number of researchers have studied Maxwell hybrid nanofluid but, so far, no researcher has delved into the effects of both thermal radiation and ohmic heating on the hydromagnetic Maxwell hybrid nanofluid yet. Therefore, this proposed study will probe into the effect of thermal radiation and ohmic heating on a hydromagnetic alumina/copper-Maxwell hybrid nanofluid over a surface stretching at a linear pace.

## **Objectives**

## **General Objective**

This study is aimed at mathematically analysing the effects of thermal radiation and ohmic heating on the



ISSN No. 2454-6194 | DOI: 10.51584/IJRIAS | Volume X Issue X October2025

hydromagnetic Al<sub>2</sub>O<sub>3</sub>/Cu-Maxwell hybrid nanofluid flow over a linearly stretching surface.

## sssSpecific Objectives

The specific objectives of this study are to;

- 1. Formulate the mathematical equations for the fluid flow in the presence of thermal radiation and ohmic heating on hydromagnetic hybrid Maxwell nanofluid flow.
- 2. Transform the equations to its non-dimensional form using appropriate similarity variables from existing literature.
- 3. Investigate the effects of volume fraction, Eckert number, magnetic field, radiation and other pertinent parameters on the flow velocity and temperature.

## Significance of the Study

The need for increased energy transmission at a minimal cost is a necessity in industries. Maxwell model is widely used in industries and making its heat transmission efficient is pivotal in polymerization. The aim of this study is to theoretically investigate the impacts that thermal radiation and ohmic heating have on the conductivity of the Maxwell hybrid nanofluid. The results of the study will provide useful information to polymeric industries on how various parameters such as radiation and magnetic parameters should be adjusted during the polymerization processes for maximum efficiency in energy transmission. The importance of this study is multifaceted and far-reaching. By advancing our understanding of energy transmission efficiency in industrial processes, it promises to deliver tangible benefists fssssssssssor industries, the environment, scientific knowledge, and education. As such, it represents a significant contribution to both academic research and practical applications, with the potential to reshape industrial practices and foster a more sustainable future.

## LITERATURE REVIEW

#### Introduction

In this section, already existing literature are discussed in the first section and the gap found is highlighted in the second section.

## **Existing Literature**

Nanotechnology is a fast growing, heat and mass transfer enhancement field that was spearheaded by Maxwell (1873). In an attempt to improve a variety of fluid features, Maxwell (1873) added solid particles in a base fluid which were millimetre in size. This upgraded the base-fluid features but had a couple of flaws that were later eliminated when Choi and Eastman (1995) proposed the use of nanoparticles instead. The proposed nanoparticles greatly refined the base-fluid properties, but, with the increasing demand for highly efficient gadgets especially electronics, the demand for a better heat transfer enhancer grew.

Suresh et al. (2011) proposed hybrid nanofluids, which, through the past decade's research, have proven to be superior in every way to the nanofluids. Hady et al. (2012) studied the impacts of radiation on a hybrid nanofluid over a sheet that is stretching at a non-linear pace. From the study, a surge in the radiation and the non-linear parameters heightened the heat rate performance. Using boundary layer analysis launched by Sakiadis (1961) and Homotopy Based Approach, Farooq et al. (2019) uncovered that, for a hydromagnetic Maxwell fluid carrying nanomaterials, increasing the Hartman and Deborah numbers boosts the flow velocity but depreciates the heat transfer performance. Rajesh et al. (2020) worked on convective MHD flow over a stretching sheet where the results showcased the superiority of hybrid nanofluids over the nanofluid.

Mutuku (2016) concurs with already existing literature on the enhancement of fluid heat transfer in the



ISSN No. 2454-6194 | DOI: 10.51584/IJRIAS | Volume X Issue X October2025

presence of nanoparticles. In their study, the use of CuO nanoparticle is found to have the most cooling effect compared to alumina and titanium oxide in Ethylene glycol. In their study, Ali et al. (2021) confirms that the addition of two-oxide nanoparticles boosts the flow temperature better than when non-oxide nanoparticles are used. Zainal et al. (2022) hails this combination for its stability. Further, Jaafar et al. (2022) points out that Alumina / Copper is not only stable, but also a good conductor and is corrosion resistant. Jaafar et al. (2022) agrees with Ali et al. (2021) and also points out that the use of Al<sub>2</sub>O<sub>3</sub> / Cu nanoparticle combination is most common since their conductivity is high and the corrosion drawback is eliminated. A duality of solutions is recorded by Jaafar et al. (2022) where one is steady and the other result is unsteady. In the analysis of the role of thermal radiation on a rotating magnetic hybrid nanofluid, Asghar et al. (2022) reports similar solutions to Jaafar et al. (2022) but rebrands the outcomes as either stable or unstable. Further, a growth in the temperature distribution is recorded when the Eckert number and the radiation parameter surge. The study conducted by Zainal et al. (2022) on role of radiation on Maxwell hybrid nanofluid in a region of stagnation records similar results as obtained by Asghar et al. (2022).

Khan et al. (2023) explores the impact of adding nanoparticles to grease by modelling the fluid behaviour using the Maxwell model. The use Maxwell base fluid here showcases the expansive applications of this model in industries since majority of the fluids commonly used display viscoelasticity. Great enhancement in heat transmission is observed with the addition of the nanoparticles in this study. Aside from the major advancement in the heating and cooling of machinery, this research boasts of friction reduction and approximately 3% mass transfer reduction as a result of the presence of nanoparticles. Wang et al. (2023) uses the Buongiorno model to further investigate the movement of nanoparticles in the Maxwell fluid under the influence of temperature gradient and Brownian motion. In the study, the interaction of thermal radiation, electromagnetic waves and chemical reactions are explored. The impacts of radiation and the occurring reactions on the flow velocity and temperature are highlighted. This study's results are found to be consistent with those observed by Khan et al. (2023). Vijay & Sharma (2023) further considered the stagnation effects, heat and mass transmission on the Maxwell nanofluid. The model is solved using finite element method and the resulting solution informs us of similar findings to what Wang et al. (2023) and Khan et al. (2023) already got.

## Comparative Analysis of Maxwell Hybrid Nanofluid Studies

## **Radiation Effects: Methodological Approaches**

Studies on thermal radiation in hybrid nanofluids have employed diverse numerical techniques with varying degrees of complexity. Hady et al. (2012) investigated radiation effects on hybrid nanofluid flow over a nonlinearly stretching sheet, revealing that increased radiation parameters enhance heat transfer rates. Their work established baseline understanding but was limited to Newtonian fluid assumptions.

The incorporation of non-Newtonian rheology marked a significant advancement. Farooq et al. (2019) employed the Homotopy Analysis Method (HAM) to study hydromagnetic Maxwell nanofluids, demonstrating that increasing Hartmann and Deborah numbers accelerates flow velocity while paradoxically reducing heat transfer efficiency. In contrast, Zainal et al. (2022) utilized similarity transformations coupled with the Runge-Kutta-Fehlberg method to analyze Maxwell hybrid nanofluids in stagnation regions, reporting enhanced temperature distributions with radiation—a finding that appears contradictory to Farooq et al. (2019). This discrepancy suggests that flow geometry and boundary conditions critically influence the radiation-heat transfer relationship.

Asghar et al. (2022) extended these investigations to rotating magnetic hybrid nanofluids using boundary layer analysis, discovering dual solutions (stable and unstable branches) and confirming that both Eckert number and radiation parameter amplify temperature distributions. Their results align with Zainal et al. (2022), suggesting that rotational effects do not fundamentally alter the radiation-temperature relationship established in non-rotating flows.



ISSN No. 2454-6194 | DOI: 10.51584/IJRIAS | Volume X Issue X October2025

## Nanoparticle Selection: Experimental vs. Theoretical Consensus

A notable convergence exists across multiple studies regarding optimal nanoparticle combinations. Mutuku (2016) experimentally demonstrated that CuO nanoparticles in ethylene glycol provide superior cooling compared to Al<sub>2</sub>O<sub>3</sub> and TiO<sub>2</sub>. However, Ali et al. (2021) theoretically established that hybrid combinations of two oxide nanoparticles outperform single-particle suspensions in temperature enhancement. This apparent contradiction is reconciled by Jaafar et al. (2022), who identified the Al<sub>2</sub>O<sub>3</sub>/Cu hybrid as optimal due to its stability, high thermal conductivity, and corrosion resistance—combining the benefits observed in both earlier studies.

Zainal et al. (2022) validated this Al<sub>2</sub>O<sub>3</sub>/Cu combination experimentally, emphasizing its long-term stability in Maxwell base fluids. The consensus across these studies (Ali et al., 2021; Jaafar et al., 2022; Zainal et al., 2022) establishes Al<sub>2</sub>O<sub>3</sub>/Cu as the industry-preferred hybrid for thermal applications, motivating its selection in the current work.

## **Dual/Multiple Solutions and Stability Analysis**

An intriguing pattern emerges regarding solution multiplicity in these systems. Jaafar et al. (2022) reported dual solutions—one steady and one unsteady—for hybrid nanofluid flow over shrinking surfaces. Asghar et al. (2022) reframed these as stable and unstable solutions, applying linear stability analysis to determine physical realizability. This methodological enhancement (stability analysis) represents a critical advancement, as it distinguishes mathematically valid solutions from physically observable ones.

The prevalence of dual solutions across studies (Jaafar et al., 2022; Asghar et al., 2022) suggests that hybrid Maxwell nanofluids under magnetic fields exhibit inherent bifurcation behavior, necessitating stability analysis in future investigations.

## **Recent Advances: Coupled Physics and Industrial Applications**

Recent investigations have increasingly focused on multi-physics coupling. Khan et al. (2023) modeled nanoparticle-enhanced grease using the Maxwell rheological framework, demonstrating not only 3% enhanced heat transfer but also significant friction reduction—a dual benefit crucial for lubrication industries. Wang et al. (2023) advanced this by incorporating the Buongiorno model to capture thermophoresis and Brownian motion, coupled with thermal radiation, electromagnetic effects, and chemical reactions. Their findings aligned with Khan et al. (2023) regarding temperature enhancement but provided deeper mechanistic insight into nanoparticle migration patterns.

Vijay & Sharma (2023) employed Finite Element Method (FEM) to investigate stagnation point flow, mass transfer, and heat transfer in Maxwell nanofluids, corroborating the temperature enhancement trends observed by Wang et al. (2023) and Khan et al. (2023). The consistency across different numerical methods (HAM, Runge-Kutta, FEM) strengthens confidence in these qualitative trends despite quantitative variations.

#### Established gap

From the review above, it is to our understanding that the investigations into the role of thermal radiation on the flow of hybrid Maxwell nanofluid over rotating surfaces, as well as shrinking and stretching surfaces, has garnered significant attention in recent research. However, there has been limited focus on understanding the impact of thermal radiation coupled with ohmic heating over a surface that linearly stretches in a magnetic hybrid Maxwell nanofluid context. The understanding of thermal radiation and ohmic heating have been found to be crucial in determining the heat insulators to be used in our gadgets and industrial machinery. Motivated to address this gap, the proposed work aims to explore the influence of thermal radiation and ohmic heating on hydromagnetic Maxwell hybrid nanofluid flow. The base fluid is Maxwell, with alumina and copper nanoparticles chosen as nanoparticles. This study seeks to provide a clearer understanding of the interactions

between heat transfer, fluid flow, and magnetic fields in such systems, offering insights valuable for various industrial applications and theoretical advancements in fluid dynamics.

## METHODOLOGY

#### Introduction

In this section, the assumptions made are presented, the flow geometry is displayed and the flow model is formulated. The model equations are then transformed into a non-dimensional system using similarity variables obtained from existing literature. The numerical techniques used to solve the resulting system of equations is then discussed.

## **Formulation of Governing Equations**

Figure 0.1: Flow geometry

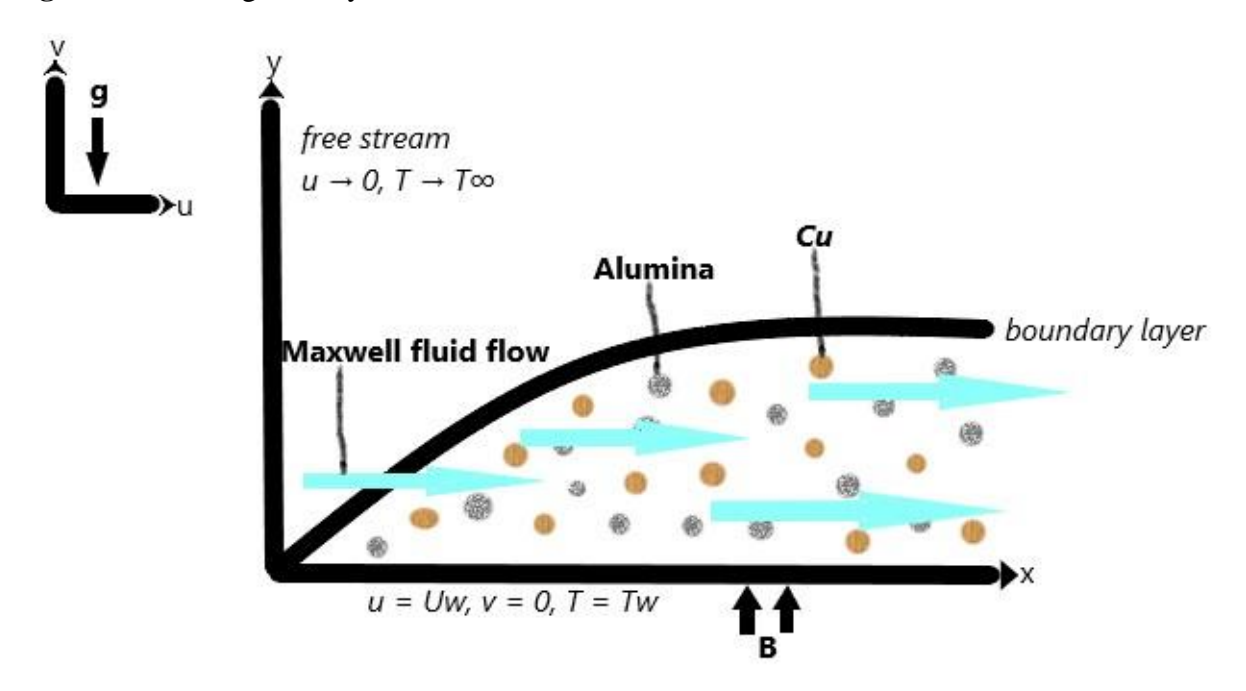


Figure (3.1) displays the 2-D, incompressible flow geometry. Here, a colloidal suspension of  $Al_2O_4/Cu$  nanoparticles in Maxwell base fluid form the hybrid nanofluid. The surface is stretching at a linear pace in the direction  $x \ge 0$ . The flow is experiencing ohmic heating, thermal radiation and a constant perpendicular magnetic field.

The following assumptions are made for the flow under consideration;

- 1. The flow is an incompressible and steady, and can be represented as a two-dimensional boundary layer flow.
- 2. The flow occurs over a linearly stretching flat surface along the x-direction, where x > 0.
- 3. A constant perpendicular magnetic field strength is applied to the flow.
- 4. The no-slip condition is obeyed on the surface.

By modifying Zainal et al. (2022) model to incorporate body forces and ohmic heating in the momentum and energy equations respectively, we have the continuity equation as;

$$\frac{\partial \mathbf{u}}{\partial \mathbf{x}} + \frac{\partial \mathbf{v}}{\partial \mathbf{y}} = \mathbf{0} \tag{3.1.1}$$

The hydromagnetic maxwell hybrid nanofluid momentum equation is given as

$$u\frac{\partial u}{\partial x} + v\frac{\partial u}{\partial y} = \mu_{\rm hnf}\rho_{\rm hnf}\frac{\partial^2 u}{\partial y^2} + 2\vartheta_f\Lambda\frac{\partial u}{\partial y}\frac{\partial^2 u}{\partial y^2} + g\beta(T - T_\infty) - \frac{\sigma_{\rm hnf}}{\rho_{\rm hnf}}B^2u \tag{3.1.2}$$

Taking into account the thermal radiation effects, the energy equation is modified to;

$$u\frac{\partial T}{\partial x} + v\frac{\partial T}{\partial y} = \frac{1}{(\rho C_p)_{hnf}} \left( \kappa_{hnf} \frac{\partial^2 T}{\partial y^2} - \frac{\partial q}{\partial y} - Q_0 (T - T_w) \right)$$
(3.1.3)

where, the radiative heat flux q is obtained from the Rosseland approximation as;

$$q = -\frac{4\sigma^*}{3k^*} \frac{\partial T^4}{\partial y}$$

From Taylor's series;

$$T^4 \approx 4T_{\infty}^3 T - 3T_{\infty}^4$$

Therefore;

$$\frac{\partial \mathbf{q}}{\partial \mathbf{y}} = -\frac{16\sigma^* \mathbf{T}_{\infty}^3}{3\mathbf{k}^*} \frac{\partial^2 \mathbf{T}}{\partial \mathbf{y}^2}.$$

The boundary equations to capture linear stretching and the no slip conditions are given as

$$u(0,x) = ax, \ v(0,x) = 0, \ T(0,x) = T_w.$$
 (3.1.4)

where  $a \ge 0$ , such that, at a = 0, the surface is immobile and at a > 0, the surface is stretching. The free stream boundary conditions are:

$$u(\infty, x) \rightarrow 0$$
,  $T(\infty, x) = T_{\infty}.(3.1.5)$ 

## **Effective properties**

The three nanoparticles, each has their thermal and electrical properties, that they contribute to the ternary hybrid nanofluid. The properties of the resulting ternary hybrid nanofluid is referred to as the effective properties. These properties have been estimated in various experimental research and models for the effective properties have been fitted using experimental data. Based on the work of Allehiany et al. (2023), the model for the effective thermal conductivity, effective electrical conductivity, effective thermal capacity, effective density and effective viscosity of the ternary hybrid nanofluid are;

$$\frac{\kappa_{\text{hnf}}}{\kappa_{\text{f}}} = \frac{2(1-\phi)\phi \,\kappa_{\text{f}} + (1+2\phi) \,\sum_{i=1}^{2} \phi_{i} \kappa_{i}}{(2+\phi)\phi \kappa_{\text{f}} + (1-\phi) \,\sum_{i=1}^{2} \phi_{i} \kappa_{i}},$$
(3.2.1)

$$\frac{\sigma_{\text{hnf}}}{\sigma_{\text{f}}} = \frac{2(1-\phi)\phi \,\sigma_{\text{f}} + (1+2\phi) \,\sum_{i=1}^{2} \phi_{i} \sigma_{i}}{(2+\phi)\phi \sigma_{\text{f}} + (1-\phi) \sum_{i=1}^{2} \phi_{i} \sigma_{i}},$$
(3.2.2)

$$\left(\rho c_{p}\right)_{hnf} = (1 - \phi)\left(\rho c_{p}\right)_{f} + \sum_{i=1}^{2} \phi_{i}\left(\rho c_{p}\right)_{i}, \tag{3.2.3}$$

$$\rho_{\text{hnf}} = (1 - \phi)\rho_f + \sum_{i=1}^2 \phi_i \rho_i, \tag{3.2.4}$$

$$\mu_{\rm hnf} = \mu_{\rm f} (1 - \phi)^{-2}. \tag{3.2.5}$$

where  $\kappa_{hnf}$  and  $\kappa_{f}$  denote the effective and base fluid thermal conductivities, respectively, and  $\phi_{i}$  represents the nanoparticle volume fraction.

Equation (3.2.1) derives from Maxwell's effective medium theory, modeling thermal conductivity enhancement from nanoparticles in base fluid. The term  $(1-\phi)\kappa_f$  represents base fluid heat transfer, while  $\phi_{i\kappa i}$  reflects nanoparticle conductive contribution. The numerator quantifies weighted enhancement; the denominator accounts for interfacial resistance and particle-fluid interactions.

Equation (3.2.2) models electrical conductivity enhancement using Maxwell's theory. Metallic nanoparticles increase conduction through electron hopping and interfacial polarization, with  $\phi_i \sigma_i$  representing nanoparticle contributions to charge transport.

Equation (3.2.3) defines hybrid nanofluid heat capacity as a weighted sum of base fluid and nanoparticle contributions, representing combined thermal energy storage capacity of the mixture.

Equation (3.2.4) expresses hybrid nanofluid density as mass-weighted average of base fluid and nanoparticle densities, accounting for volume fraction of each component in the suspension.

Equation (3.2.5) describes viscosity increase due to nanoparticle suspension. The factor  $(1-\phi)^{-2}$  reflects empirical correlations for flow resistance enhancement from uniformly dispersed particles.

and for the sake of simplicity, we rewrite the models as

$$\frac{\kappa_{hnf}}{\kappa_f} = \frac{2(1-\varphi)\varphi\kappa_f + (1+2\varphi)\Sigma_{i=1}^2 \varphi_i \kappa_i}{(2+\varphi)\varphi\kappa_f + (1-\varphi)\Sigma_{i=1}^2 \varphi_i \kappa_i} = A_1 \Rightarrow \kappa_{hnf} = A_1 \kappa_f$$

$$(3.2.6)$$

$$\frac{\sigma_{\text{hnf}}}{\sigma_{\text{f}}} = \frac{2(1 - \phi)\phi\sigma_{\text{f}} + (1 + 2\phi)\Sigma_{\text{i=1}}^{2}\phi_{\text{i}}\sigma_{\text{i}}}{(2 + \phi)\phi\sigma_{\text{f}} + (1 - \phi)\Sigma_{\text{i=1}}^{2}\phi_{\text{i}}\sigma_{\text{i}}} = A_{2} \Rightarrow \sigma_{\text{hnf}} = A_{2}\sigma_{\text{f}}$$
(3.2.7)

$$\left(\rho c_{p}\right)_{hnf} = (1 - \phi)\left(\rho c_{p}\right)_{f} + \sum_{i=1}^{2} \phi_{i}\left(\rho c_{p}\right)_{i}$$



$$= \left(1 - \phi + \frac{1}{\left(\rho c_{p}\right)_{f}} \sum_{i=1}^{2} \phi_{i} \left(\rho c_{p}\right)_{i}\right) \left(\rho c_{p}\right)_{f}$$

$$= A_{3} \left(\rho c_{p}\right)_{f}$$
(3.2.8)

$$\rho_{hnf} = (1 - \phi)\rho_f + \sum_{i=1}^2 \phi_i \rho_i = \left(1 - \phi + \frac{1}{\rho_f} \sum_{i=1}^2 \phi_i \rho_i\right) \rho_f = A_4 \rho_f$$
 (3.2.9)  

$$\mu_{hnf} = 0.904 e^{0.148\phi} \mu_f = A_5 \mu_f$$
 (3.2.10)

Equation (3.2.6) simplifies thermal conductivity ratio as enhancement factor A<sub>1</sub>, encapsulating nanoparticle contributions into a compact coefficient multiplying base fluid conductivity.

Equation (3.2.7) simplifies electrical conductivity ratio as enhancement factor A<sub>2</sub>, condensing nanoparticle effects into a multiplicative term for streamlined analysis.

Equation (3.2.8) rewrites heat capacity as  $A_3(\rho cp)f$ , where  $A_3$  represents the normalized enhancement factor from nanoparticle thermal storage contributions.

Equation (3.2.9) expresses density as A<sub>4</sub>ρf, where A<sub>4</sub> captures mass-weighted contribution of nanoparticles, simplifying density calculations in governing equations.

Equation (3.2.10) correlates viscosity using empirical formula with exponential dependence on volume fraction  $\phi$ , defining enhancement factor A<sub>5</sub> for flow resistance.

## **Similarity Transformation**

The flow model (3.1.1 -3.1.5) will be transformed to a non-dimensional system of ordinary differential equations using similarity variables

$$\eta = ya^{\frac{1}{2}}\theta_f^{-\frac{1}{2}}, \quad u = ax\frac{d}{d\eta}f(\eta), \quad v = -a^{\frac{1}{2}}\theta_f^{\frac{1}{2}}f(\eta), \quad T = T_{\infty} + (T_w - T_{\infty})\Theta(\eta).$$
 (3.3.1)

The shooting technique will be employed in the conversion of the resulting dimensionless boundary conditions to their equivalent initial conditions. The shooting technique is used because the method of solution of the resulting ODEs will be numerical techniques. Solving BVPs using numerical techniques is difficult and borderline impossible sometimes, therefore, the shooting technique assists in overcoming this setback. The resulting IVP's approximate solutions will be obtained using RK in MATLAB bvp4c solver. The results will be presented as graphs. The outcomes will be analysed and discussed. Conclusions will be drawn from the study results and suitable recommendations will be presented.

Since  $\eta$  is a function of y only, then  $\eta_y = a^{\frac{1}{2}} \vartheta_f^{-\frac{1}{2}}$  and  $\eta_x = 0$ . The first partial derivatives of u with respect to x and y are found as follows;

$$\begin{split} \frac{\partial u}{\partial x} &= \frac{d}{dx} \left( ax \frac{d}{d\eta} f(\eta) \right) = a \frac{d}{d\eta} f(\eta) \frac{d}{dx}(x) = a \frac{d}{d\eta} f(\eta) \\ \frac{\partial u}{\partial y} &= \frac{d}{d\eta} \left( ax \frac{d}{d\eta} f(\eta) \right) \frac{d\eta}{dy} \\ &= ax \frac{d}{d\eta} \left( \frac{d}{d\eta} f(\eta) \right) \frac{d\eta}{dy} \end{split}$$



$$= ax \frac{d^2}{dn^2} f(\eta) \frac{d\eta}{dv}$$
 (3.3.3)

These equations apply the chain rule to transform partial derivatives from Cartesian (x,y) to similarity variable  $\eta$ , simplifying boundary layer equations through coordinate transformation.

The second partial derivative of u with respect to y is as follows;

$$\begin{split} \frac{\partial^2 u}{\partial y^2} &= \frac{\partial}{\partial y} \left( \frac{\partial u}{\partial y} \right) = \frac{\partial}{\partial y} \left( ax \frac{d^2}{d\eta^2} f(\eta) \frac{d\eta}{dy} \right) \\ &= \frac{d}{d\eta} \left( ax \frac{d^2}{d\eta^2} f(\eta) \frac{d\eta}{dy} \right) \frac{d\eta}{dy} \\ &= ax \frac{d^3}{d\eta^3} f(\eta) \left( \frac{d\eta}{dy} \right)^2 \end{split} \tag{3.3.4}$$

Second derivative transformation using chain rule twice, converting  $\partial^2 u/\partial y^2$  from Cartesian to similarity coordinates, yielding third-order derivative in  $\eta$  with squared transformation factor.

Next is to consider the first partial derivatives of the variable v with respect x and y are as follows;

$$\begin{split} \frac{\partial v}{\partial x} &= 0\\ \frac{\partial v}{\partial y} &= \frac{\partial}{\partial y} \left( -a^{\frac{1}{2}} \vartheta_f^{\frac{1}{2}} \frac{d}{d\eta} f(\eta) \right) = \frac{\partial}{\partial y} \left( -a^{\frac{1}{2}} \vartheta_f^{\frac{1}{2}} \frac{d}{d\eta} f(\eta) \right) \frac{d\eta}{dy} \\ &= -a^{\frac{1}{2}} \vartheta_f^{\frac{1}{2}} \frac{d}{d\eta} f(\eta) \frac{d\eta}{dy}. \end{split} \tag{3.3.5}$$

Partial derivatives of velocity component v:  $\partial v/\partial x$  vanishes identically, while  $\partial v/\partial y$  transforms through chain rule, introducing fractional powers and transformation coefficient  $d\eta/dy$ .

The second partial derivative of v with respect to y is as follows;

$$\begin{split} \frac{\partial^{2} v}{\partial y^{2}} &= \frac{\partial}{\partial y} \left( \frac{\partial v}{\partial y} \right) = \frac{\partial}{\partial y} \left( -a^{\frac{1}{2}} \vartheta_{f}^{\frac{1}{2}} \frac{d}{d\eta} f(\eta) \frac{d\eta}{dy} \right) \\ &= \frac{d}{d\eta} \left( -a^{\frac{1}{2}} \vartheta_{f}^{\frac{1}{2}} \frac{d}{d\eta} f(\eta) \frac{d\eta}{dy} \right) \frac{d\eta}{dy} \\ &= -a^{\frac{1}{2}} \vartheta_{f}^{\frac{1}{2}} \frac{d}{d\eta} \left( \frac{d}{d\eta} f(\eta) \frac{d\eta}{dy} \right) \frac{d\eta}{dy} \\ &= -a^{\frac{1}{2}} \vartheta_{f}^{\frac{1}{2}} \frac{d^{2}}{d\eta^{2}} f(\eta) \left( \frac{d\eta}{dy} \right)^{2} \end{split}$$
(3.3.6)

The temperature T is a function of  $\Theta$  which is a function of  $\eta$  and as a result, T is independent of x. The partial derivative of T with respect to x is zero so that

$$\frac{\partial \mathbf{T}}{\partial \mathbf{x}} = 0,$$

and the partial derivatives of T with respect to y is obtained as



$$\begin{split} \frac{\partial T}{\partial y} &= \frac{\partial}{\partial y} \left( T_{\infty} + (T_{w} - T_{\infty}) \Theta(\eta) \right) = (T_{w} - T_{\infty}) \frac{d}{d\eta} \left( \Theta(\eta) \right) \frac{d\eta}{dy} \\ \frac{\partial^{2} T}{\partial y^{2}} &= \frac{\partial}{\partial y} \left( \frac{\partial T}{\partial y} \right) = \frac{\partial}{\partial y} \left( (T_{w} - T_{\infty}) \frac{d}{d\eta} \left( \Theta(\eta) \right) \frac{d\eta}{dy} \right) \\ &= (T_{w} - T_{\infty}) \frac{\partial}{\partial y} \left( \frac{d}{d\eta} \left( \Theta(\eta) \right) \frac{d\eta}{dy} \right) \\ &= (T_{w} - T_{\infty}) \frac{d}{d\eta} \left( \frac{d}{d\eta} \left( \Theta(\eta) \right) \frac{d\eta}{dy} \right) \frac{d\eta}{dy} \\ &= (T_{w} - T_{\infty}) \frac{d^{2}}{d\eta^{2}} \left( \Theta(\eta) \right) \left( \frac{d\eta}{dy} \right)^{2} \end{split} \tag{3.3.7}$$

Temperature derivatives transform from Cartesian to similarity coordinates. First derivative  $\partial T/\partial y$  and second derivative  $\partial^2 T/\partial y^2$  involve temperature difference (Tw - T $\infty$ ), dimensionless function  $\Theta(\eta)$ , and transformation factor  $d\eta/dy$ .

By substituting  $\eta_v$  we have

$$\frac{\partial u}{\partial x} = a \frac{d}{d\eta} f(\eta)$$

$$\frac{\partial u}{\partial y} = ax \frac{d^2}{d\eta^2} f(\eta) \frac{d\eta}{dy}$$

$$= ax \frac{d^2}{d\eta^2} f(\eta) \left( a^{\frac{1}{2}} \theta_f^{-\frac{1}{2}} \right)$$

$$= ax \left( a^{\frac{1}{2}} \theta_f^{-\frac{1}{2}} \right) \frac{d^2}{d\eta^2} f(\eta)$$

$$= x \sqrt{\frac{a^3}{\theta_f}} \frac{d^2}{d\eta^2} f(\eta)$$

$$= x \sqrt{\frac{\theta^3}{\theta_f}} \frac{d^2}{d\eta^2} f(\eta)$$

$$= ax \frac{d^3}{d\eta^3} f(\eta) \left( \frac{d\eta}{dy} \right)^2$$

$$= ax \frac{d^3}{d\eta^3} f(\eta) \left( a^{\frac{1}{2}} \theta_f^{-\frac{1}{2}} \right)^2$$

$$= \frac{a^2 x}{\theta} \frac{d^3}{d\eta^3} f(\eta)$$

$$\frac{\partial v}{\partial y} = 0$$

$$\frac{\partial v}{\partial y} = -a^{\frac{1}{2}} \theta_f^{\frac{1}{2}} \frac{d}{d\eta} f(\eta) \frac{d\eta}{dy}$$

$$= -a^{\frac{1}{2}} \theta_f^{\frac{1}{2}} \frac{d}{d\eta} f(\eta) \left( a^{\frac{1}{2}} \theta_f^{-\frac{1}{2}} \right)$$

$$= -a \frac{d}{d\eta} f(\eta). \qquad (3.3.10)$$

$$\frac{\partial^2 v}{\partial v^2} = -a^{\frac{1}{2}} \theta_f^{\frac{1}{2}} \frac{d^2}{d\eta^2} f(\eta) \left( \frac{d\eta}{dv} \right)^2$$



$$= -a^{\frac{1}{2}} \vartheta_{f}^{\frac{1}{2}} \frac{d^{2}}{d\eta^{2}} f(\eta) \left( a^{\frac{1}{2}} \vartheta_{f}^{-\frac{1}{2}} \right)^{2}$$

$$= -\sqrt{\frac{a^{3}}{\vartheta_{f}}} \frac{d^{2}}{d\eta^{2}} f(\eta). \tag{3.3.11}$$

$$\begin{split} \frac{\partial T}{\partial y} &= (T_w - T_\infty) \frac{d}{d\eta} \Theta(\eta) \frac{d\eta}{dy} \\ &= (T_w - T_\infty) \left( a^{\frac{1}{2}} \vartheta_f^{-\frac{1}{2}} \right) \frac{d}{d\eta} \Theta(\eta). \end{split} \tag{3.3.12}$$

$$\begin{split} \frac{\partial^2 T}{\partial y^2} &= (T_w - T_\infty) \frac{d^2}{d\eta^2} \big( \Theta(\eta) \big) \Big( \frac{d\eta}{dy} \Big)^2 \\ &= \frac{a (T_w - T_\infty)}{\vartheta} \frac{d^2}{d\eta^2} \big( \Theta(\eta) \big) \end{split} \tag{3.3.13}$$

Equations (3.3.8)-(3.3.9): Substituting similarity variable  $\eta y$  yields simplified velocity derivatives.  $\partial u/\partial y$  combines transformation factors, while  $\partial^2 u/\partial y^2$  becomes  $a^2 x/\vartheta$  times third derivative in  $\eta$ -space.

Equations (3.3.10)-(3.3.11): Transverse velocity derivatives:  $\partial v/\partial x$  vanishes,  $\partial v/\partial y$  simplifies to  $-a \cdot d/d\eta \cdot f(\eta)$ , and  $\partial^2 v/\partial y^2$  reduces to negative square root term involving kinematic viscosity  $\vartheta$ .

Equations (3.3.12)-(3.3.13): Temperature derivatives after substitution:  $\partial T/\partial y$  contains temperature difference and transformation factor;  $\partial^2 T/\partial y^2$  simplifies to  $a(Tw-T\infty)/\vartheta$  times second derivative of dimensionless temperature  $\Theta(\eta)$ .

Consider the left hand side of equation (3.1.2) and we have

$$\begin{split} LHS &= u \frac{\partial u}{\partial x} + v \frac{\partial u}{\partial y} \\ &= \left( ax \frac{d}{d\eta} f(\eta) \right) \left( a \frac{d}{d\eta} f(\eta) \right) + \left( -a^{\frac{1}{2}} \vartheta_f^{\frac{1}{2}} f(\eta) \right) \left( x \sqrt{\frac{a^3}{\vartheta_f}} \frac{d^2}{d\eta^2} f(\eta) \right) \\ &= (a^2 x) \left( \frac{d}{d\eta} f(\eta) \right)^2 + (-a^2 x) f(\eta) \frac{d^2}{d\eta^2} f(\eta) \\ &= a^2 x \left( \left( \frac{d}{d\eta} f(\eta) \right)^2 - f(\eta) \frac{d^2}{d\eta^2} f(\eta) \right) \end{split} \tag{3.3.14}$$

Left-hand side of momentum equation transforms by substituting velocity derivatives, combining convective terms  $u\partial u/\partial x$  and  $v\partial u/\partial y$  into simplified expression involving first and second derivatives in  $\eta$ -coordinates.

Next is the right hand side of equation (3.1.2) and we have

$$RHS = \frac{\mu_{hnf}}{\rho_{hnf}} \left( \frac{\partial^2 u}{\partial y^2} \right) \ + \ 2\vartheta_f \Lambda \left( \frac{\partial u}{\partial y} \right) \left( \frac{\partial^2 u}{\partial y^2} \right) + \ g\beta \big( T - T_{infty} \big) \ - \ \left( \frac{\sigma_{hnf}}{\rho_{hnf}} \right) B^2 u$$



$$\begin{split} &=\frac{\mu_{\mathrm{hnf}}}{\rho_{\mathrm{hnf}}}\bigg(\frac{a^{2}x}{\vartheta_{\mathrm{f}}}\frac{d^{3}f(\eta)}{d\eta^{3}}\bigg)+2\vartheta_{\mathrm{f}}\Lambda x\Bigg(\sqrt{\frac{a^{3}}{\vartheta_{\mathrm{f}}}}\bigg)\frac{d^{2}f(\eta)}{d\eta^{2}}\frac{a^{2}x}{\vartheta_{\mathrm{f}}}\frac{d^{3}f(\eta)}{d\eta^{3}}+g\beta(T_{\mathrm{w}}-T_{\infty})\Theta(\eta)\\ &-\frac{\sigma_{\mathrm{hnf}}}{\rho_{\mathrm{hnf}}}B^{2}\Bigg(ax\frac{d}{d\eta}f(\eta)\Bigg),\\ &=a^{2}x\Bigg(\frac{\mu_{\mathrm{hnf}}}{\rho_{\mathrm{hnf}}\vartheta_{\mathrm{f}}}\frac{d^{3}f(\eta)}{d\eta^{3}}+2\Lambda ax\sqrt{\frac{a}{\vartheta_{\mathrm{f}}}}\frac{d^{2}f(\eta)}{d\eta^{2}}\frac{d^{3}f(\eta)}{d\eta^{3}}+\frac{g\beta(T_{\mathrm{w}}-T_{\infty})}{a^{2}x}\Theta(\eta)\\ &-\frac{\sigma_{\mathrm{hnf}}}{a\rho_{\mathrm{hnf}}}B^{2}\frac{d}{d\eta}f(\eta)\Bigg). \end{split} \tag{3.3.15}$$

Right-hand side of momentum equation transforms by substituting derivatives, incorporating viscous diffusion, Darcy-Forchheimer porous terms, thermal buoyancy, and magnetic field effects into simplified  $\eta$ -coordinate expression with nanofluid properties.

Combining the left and right hand sides and equation (3.1.2) becomes

$$\begin{split} a^2x \Biggl(\Biggl(\frac{d}{d\eta}f(\eta)\Biggr)^2 - f(\eta)\frac{d^2}{d\eta^2}f(\eta)\Biggr) \\ &= a^2x \Biggl(\frac{\mu_{hnf}}{\rho_{hnf}\theta_f}\frac{d^3f(\eta)}{d\eta^3} + 2\Lambda ax \sqrt{\frac{a}{\theta_f}}\frac{d^2f(\eta)}{d\eta^2}\frac{d^3f(\eta)}{d\eta^3} + \frac{g\beta(T_w - T_\infty)}{a^2x}\Theta(\eta) \\ &- \frac{\sigma_{hnf}}{a\rho_{hnf}}B^2\frac{d}{d\eta}f(\eta)\Biggr) \\ \Biggl(\frac{d}{d\eta}f(\eta)\Biggr)^2 - f(\eta)\frac{d^2}{d\eta^2}f(\eta) \\ &= \frac{\mu_{hnf}}{\rho_{hnf}\theta_f}\frac{d^3f(\eta)}{d\eta^3} + 2\Lambda ax \sqrt{\frac{a}{\theta_f}}\frac{d^2f(\eta)}{d\eta^2}\frac{d^3f(\eta)}{d\eta^3} + \frac{g\beta(T_w - T_\infty)}{a^2x}\Theta(\eta) \\ &- \frac{\sigma_{hnf}}{a\rho_{hnf}}B^2\frac{d}{d\eta}f(\eta) \end{aligned} \tag{3.3.17}$$

Combining left and right sides yields transformed momentum equation in  $\eta$ -coordinates, balancing convective acceleration with viscous diffusion, porous medium resistance, thermal buoyancy, and magnetic damping effects.

Simplified momentum equation balances inertial terms with viscous diffusion, Darcy-Forchheimer porous resistance, thermal buoyancy force, and Lorentz magnetic force in dimensionless similarity coordinates.

Now, by using equations (3.2.7) and (3.2.9), we have

$$\frac{\sigma_{\rm hnf}}{a\rho_{\rm hnf}} = \frac{A_2\sigma_{\rm f}}{aA_4\rho_{\rm f}}, \frac{\mu_{\rm hnf}}{\rho_{\rm hnf}\vartheta_{\rm f}} = \frac{A_5\mu_{\rm f}}{A_4\rho_{\rm f}\vartheta_{\rm f}} = \frac{A_5}{A_4}$$
(3.3.18)



and the momentum equation becomes

$$\left(\frac{\mathrm{d}f}{\mathrm{d}\eta}\right)^2 - f\frac{\mathrm{d}^2f}{\mathrm{d}\eta^2} = \frac{A_5}{A_4}\frac{\mathrm{d}^3f}{\mathrm{d}\eta^3} + 2\Lambda ax \sqrt{\frac{a}{\vartheta_f}}\frac{\mathrm{d}^3f}{\mathrm{d}\eta^3}\frac{\mathrm{d}^2f}{\mathrm{d}\eta^2} + \frac{g\beta(T_w - T_\infty)}{a^2x}\Theta - \frac{A_2\sigma_f}{aA_4\rho_f}B^2\left(\frac{\mathrm{d}f}{\mathrm{d}\eta}\right)$$

which is the same as

$$\begin{split} &\frac{A_5}{A_4}\frac{d^3f}{d\eta^3} + 2\Lambda ax\sqrt{\frac{a}{\vartheta_f}}\frac{d^3f}{d\eta^3}\frac{d^2f}{d\eta^2} - \left(\frac{df}{d\eta}\right)^2 + f\frac{d^2f}{d\eta^2} + \frac{g\beta(T_w - T_\infty)}{a^2x}\Theta - \frac{A_2\sigma_f}{aA_4\rho_f}B^2\left(\frac{df}{d\eta}\right) = 0\\ &\left(\frac{A_5}{A_4} + 2\Lambda ax\sqrt{\frac{a}{\vartheta_f}}\frac{d^2f}{d\eta^2}\right)\frac{d^3f}{d\eta^3} - \left(\frac{df}{d\eta}\right)^2 + f\frac{d^2f}{d\eta^2} + \frac{g\beta(T_w - T_\infty)}{a^2x}\Theta - \frac{A_2\sigma_f}{aA_4\rho_f}B^2\left(\frac{df}{d\eta}\right) = 0\\ &\left(\frac{A_5}{A_4} + 2We\frac{d^2f}{d\eta^2}\right)\frac{d^3f}{d\eta^3} - \left(\frac{df}{d\eta}\right)^2 + f\frac{d^2f}{d\eta^2} + Gr\Theta - \frac{A_2}{A_4}M\frac{df}{d\eta} = 0 \end{split} \tag{3.3.19}$$

Using enhancement factor ratios simplifies momentum equation into dimensionless form with coefficients A<sub>5</sub>/A<sub>4</sub>, introducing Weissenberg number (We), Grashof number (Gr), and magnetic parameter (M) for compact representation.

where

$$We = \Lambda ax \sqrt{\frac{a}{\vartheta_f}}, \ Gr = \frac{g\beta(T_w - T_\infty)}{a^2x}, \ M = \frac{\sigma_f B^2}{a\rho_f}.$$

Next stage is to consider the energy equation (3.1.3)

$$u\frac{\partial T}{\partial x} + v\frac{\partial T}{\partial y} - \frac{1}{\left(\rho c_{p}\right)_{hnf}} \left(\kappa_{hnf} \frac{\partial^{2} T}{\partial y^{2}} + \frac{16\sigma^{*} T_{\infty}^{3}}{3k^{*}} \frac{\partial^{2} T}{\partial y^{2}} - Q_{0}(T - T_{w})\right) = 0$$
(3.3.20)

and on substitutions, we have

$$\begin{split} 0 - & \left(a^{\frac{1}{2}} \vartheta_f^{\frac{1}{2}} f(\eta)\right) \left(a^{\frac{1}{2}} \vartheta_f^{-\frac{1}{2}} (T_w - T_\infty) \frac{d}{d\eta} \Theta(\eta)\right) - \frac{1}{\left(\rho c_p\right)_{hnf}} \left(\kappa_{hnf} + \frac{16\sigma^* T_\infty^3}{3k^*}\right) \frac{a(T_w - T_\infty)}{\vartheta_f} \frac{d^2}{d\eta^2} \Theta(\eta) \\ & + \frac{Q_0(T_w - T_\infty)}{\left(\rho c_p\right)_{hnf}} (\Theta - 1) = 0, \\ - & \left(f(\eta) \frac{d}{d\eta} \Theta(\eta)\right) - \left(\frac{\kappa_{hnf}}{\left(\rho c_p\right)_{hnf}} + \frac{16\sigma^* T_\infty^3}{3k^* \left(\rho c_p\right)_{hnf}}\right) \frac{1}{\vartheta_f} \frac{d^2}{d\eta^2} \Theta(\eta) + \frac{Q_0(\Theta - 1)}{a\left(\rho c_p\right)_{hnf}} = 0. \end{split}$$

Weissenberg number (We) measures viscoelastic effects, Grashof number (Gr) represents buoyancy-driven flow, and magnetic parameter (M) quantifies electromagnetic damping strength in the system.

Energy equation (3.3.20): Energy equation balances convective heat transfer with thermal conduction (including radiation effects) and heat generation/absorption, transformed into similarity coordinates using temperature and velocity derivatives.

Substituting equations (3.2.6) and (3.2.8)



$$-\left(f(\eta)\frac{d}{d\eta}\Theta(\eta)\right) - \left(\frac{A_1\kappa_f}{A_3(\rho c_p)_f\vartheta_f} + \frac{16\sigma^*T_\infty^3}{3k^*A_3(\rho c_p)_f\vartheta_f}\right)\frac{d^2}{d\eta^2}\Theta(\eta) + \frac{Q_0(\Theta - 1)}{aA_3(\rho c_p)_f} = 0. \quad (3.3.21)$$

Recall that the thermal diffusivity  $\alpha_f$  of the base fluid is defined as  $\alpha_f = \frac{\kappa_f}{(\rho c_p)_f}$  and so the equation becomes

$$-\left(f(\eta)\frac{d}{d\eta}\Theta(\eta)\right) - \left(\frac{A_1\alpha_f}{A_3\vartheta_f} + \frac{16\sigma^*T_\infty^3}{3k^*A_3\left(\rho c_p\right)_f\vartheta_f}\right)\frac{d^2}{d\eta^2}\Theta(\eta) + \frac{Q_0(\Theta-1)}{aA_3\left(\rho c_p\right)_f} = 0. \tag{3.3.22}$$

Substituting enhancement factors and thermal diffusivity definition ( $\alpha f = \kappa f/(\rho cp)f$ ) simplifies energy equation into compact dimensionless form with ratios  $A_1/A_3$ , incorporating radiation and heat generation effects.

Also setting

$$\frac{1}{\text{Pr}} = \frac{\alpha_f}{\vartheta_f}, \quad R = \frac{4\sigma^* T_{\infty}^3}{k^* \vartheta_f (\rho c_p)_f} \quad \text{ and } \quad Q = \frac{Q_0}{a (\rho c_p)_f}$$

we have

$$\begin{split} &-\left(f(\eta)\frac{d}{d\eta}\Theta(\eta)\right)-\left(\frac{A_1}{A_3Pr}+\frac{4}{3}R\right)\frac{d^2}{d\eta^2}\Theta(\eta)+\frac{Q}{A_3}(\Theta-1)=0,\\ &\left(\frac{A_1}{A_3Pr}+\frac{4}{3}R\right)\frac{d^2}{d\eta^2}\Theta(\eta)+\left(f(\eta)\frac{d}{d\eta}\Theta(\eta)\right)-\frac{Q}{A_3}(\Theta-1)=0 \end{split} \tag{3.3.23}$$

Prandtl number (1/Pr =  $\alpha f/\vartheta f$ ), radiation parameter (R), and heat generation parameter (Q) transforms energy equation into simplified form with  $A_1/A_3$  ratios.

Finally, we consider the boundary conditions. Based on the choice of the similarity variables as  $\eta = ya^{\frac{1}{2}}\theta_f^{-\frac{1}{2}}$ , we have

at 
$$y = 0$$
,  $\eta = 0$  and as  $y \to \infty$ ,  $\eta \to \infty$ .

Starting at the wall where y = 0,

$$\begin{array}{lll} u(0,x)=ax & \Rightarrow & \dfrac{df}{d\eta}=1 & \text{at } \eta=0 \\ v(0,x)=0 & \Rightarrow & f=1 & \text{at } \eta=0 \\ T(0,x)=T_w & \Rightarrow & \Theta=1 & \text{at } \eta=0 \end{array}$$

At the free stream,

$$u(\infty, x) \to 0$$
  $\Rightarrow$   $f' \to 0$  as  $\eta \to \infty$   
 $T(\infty, x) \to T_{\infty}$   $\Rightarrow$   $\Theta \to 0$  as  $\eta \to \infty$ 

Boundary conditions transform using similarity variable  $\eta$ . At wall (y=0,  $\eta$ =0): velocity matches stretching, no-penetration, and isothermal conditions. At free stream ( $\eta \rightarrow \infty$ ): velocity and temperature gradients vanish.

The dimensionless equations are therefore



$$\left(\frac{A_5}{A_4} + 2We \frac{d^2f}{d\eta^2}\right) \frac{d^3f}{d\eta^3} - \left(\frac{df}{d\eta}\right)^2 + f\frac{d^2f}{d\eta^2} + Gr\Theta - \frac{A_2}{A_4}M\frac{df}{d\eta} = 0$$
 (3.3.24)

$$\left(\frac{A_1}{A_3 Pr} + \frac{4}{3}R\right) \frac{d^2}{d\eta^2} \Theta(\eta) + f(\eta) \frac{d}{d\eta} \Theta(\eta) - \frac{Q}{A_3} (\Theta - 1) = 0$$
(3.3.25)

with the condition

$$f = 0$$
,  $\frac{df}{d\eta} = 1$ ,  $\Theta = 1$  at  $\eta = 0$  (3.3.26)  
 $f' \to 0$ ,  $\Theta \to 0$  as  $\eta \to \infty$  (3.3.27)

$$f' \to 0$$
,  $\Theta \to 0$  as  $\eta \to \infty$  (3.3.27)

where

We = 
$$\Lambda ax \sqrt{\frac{a}{\vartheta_f}}$$
,  $Gr = \frac{g\beta(T_w - T_\infty)}{a^2x}$ ,  $M = \frac{\sigma_f B^2}{a\rho_f}$  (3.3.28)

$$\alpha_{\rm f} = \frac{\kappa_{\rm f}}{\left(\rho c_{\rm p}\right)_{\rm f}}, \quad \frac{1}{\rm Pr} = \frac{\alpha_{\rm f}}{\vartheta_{\rm f}}, \quad R = \frac{4\sigma^* T_{\infty}^3}{k^* \vartheta_{\rm f} \left(\rho c_{\rm p}\right)_{\rm f}}, \quad Q = \frac{Q_0}{a \left(\rho c_{\rm p}\right)_{\rm f}}$$
 (3.3.29)

Dimensionless governing equations (3.3.24-3.3.25) couple momentum and energy with boundary conditions (3.3.26-3.3.27). Parameters We, Gr, M, Pr, R, Q characterize viscoelasticity, buoyancy, magnetism, thermal diffusion, radiation, and heat generation respectively.

## **Thermophysical Properties**

The nanoparticles under study are that made from Al<sub>2</sub>O<sub>3</sub> and Cu and the choice of base-fluid is molten polyethylene (a Maxwell fluid). The thermophysical properties of the base-fluid and that of the nanoparticles are obtained from literature and are recorded in table (3.1).

**Table 3.1**: Thermophysical properties

	к	ρ	c <sub>p</sub>	$\rho c_p$	μ
$Al_2O_3$	40	3970	765	3037050	-
Cu	400	8933	385	3439205	-
molten polyethylene	0.253	1115	2430	2709450	18.376

By substituting these values into equations (3.2.6 - 3.2.9), we have the following

$$\begin{split} A_1 &= \frac{0.506(1-\varphi)\varphi + (1+2\varphi)(34.5\varphi_1 + 1.2\varphi_2)}{0.253(2+\varphi)\varphi + (1-\varphi)(34.5\varphi_1 + 1.2\varphi_2)},\\ A_2 &= \frac{21.4(1-\varphi)\varphi \times 10^{-5} + (1+2\varphi)(6.3\varphi_1 + 4.25\varphi_2) \times 10^7}{10.7(2+\varphi)\varphi \times 10^{-5} + (1-\varphi)(6.3\varphi_1 + 4.25\varphi_2) \times 10^7},\\ A_3 &= 1-\varphi + \frac{(2011147\varphi_1 + 1546600\varphi_2)}{2709450},\\ A_4 &= 1-\varphi + \frac{(5060\varphi_1 + 2200\varphi_2)}{1115}. \end{split}$$

Substituting nanoparticle properties into equations (3.2.6-3.2.9) yields explicit enhancement factors A<sub>1</sub> through



A<sub>4</sub>, representing thermal conductivity, electrical conductivity, heat capacity, and density modifications from nanoparticle volume fractions  $\phi_1$  and  $\phi_2$ .

#### **Numerical Procedure**

The coupled PDEs governing the MHD flow of hybrid nanofluid is reformulated as a coupled system of ODEs through the use of similarity transformation. The resulting the ODEs comes with some boundary conditions at the free stream and some initial conditions at the boundary layer. This kind of problem cannot be solved by simply adopting a numerical procedure due to the inclusion of boundary conditions. The problem concerning the boundary conditions is solved by bringing in the method of Shooting Technique; which seeks the initial condition that best satisfies the boundary condition. The Runge Kutta method is used to solve the coupled ODEs with the initial conditions. The numerical results are graphed and the results are discussed herewith.

### **Analysis of Results**

#### Introduction

The parameters that emerged from the nondimensionalisation process are varied to simulate the flow. By varying a parameter while fixing other parameters, the profiles for velocity and temperature of the flow are plotted against the dimensionless distance  $\eta$ . In any case a parameter is fixed, the following values are chosen as the default for the parameters;

We = 0.1, Gr = 1, M = 2, Pr = 7, Q = 0.21, R = 0.1, 
$$\phi_1 = \phi_2 = 0.1$$
.

Recall that the flow velocity is similar to f' and temperature is similar to  $\Theta$ , hence, in the following discussion, the same notations shall be retained for these flow properties.

## RESULTS AND DISCUSSION

The parameters that emerged from the nondimensionalisation process are varied to simulate the flow. By varying a parameter while fixing other parameters, the profiles for velocity and temperature of the flow are plotted against the dimensionless distance  $\eta$ . In any case a parameter is fixed, the following values are chosen as the default for the parameters:

We = 0.1, Gr = 1, M = 2, Pr = 7, Q = 0.21, R = 0.1, 
$$\varphi_1 = \varphi_2 = 0.1$$
.

Recall that the flow velocity is similar to f' and temperature is similar to  $\Theta$ , hence, in the following discussion, the same notations shall be retained for these flow properties.

## **Effect of Grashof Number**

The Grashof number Gr measures the ratio of buoyancy to viscous forces, often arising in natural convection and defined in this study as

$$Gr = \frac{g\beta(T_w - T_\infty)}{a^2x}.$$

The behaviour of temperature with increasing Grashof number is shown in figure (4.1) while the behaviour of velocity is illustrated in figure (4.2). The figures illustrated a decrease in temperature and an increase in velocity with Grashof number. A rise in Grashof number is a consequence of increasing buoyancy force which enhances flow velocity but reduces thermal boundary layer. Hence, as Grashof number rises, temperature goes down and velocity goes up.

Figure 4.1: Effects of temperature to Grashof number



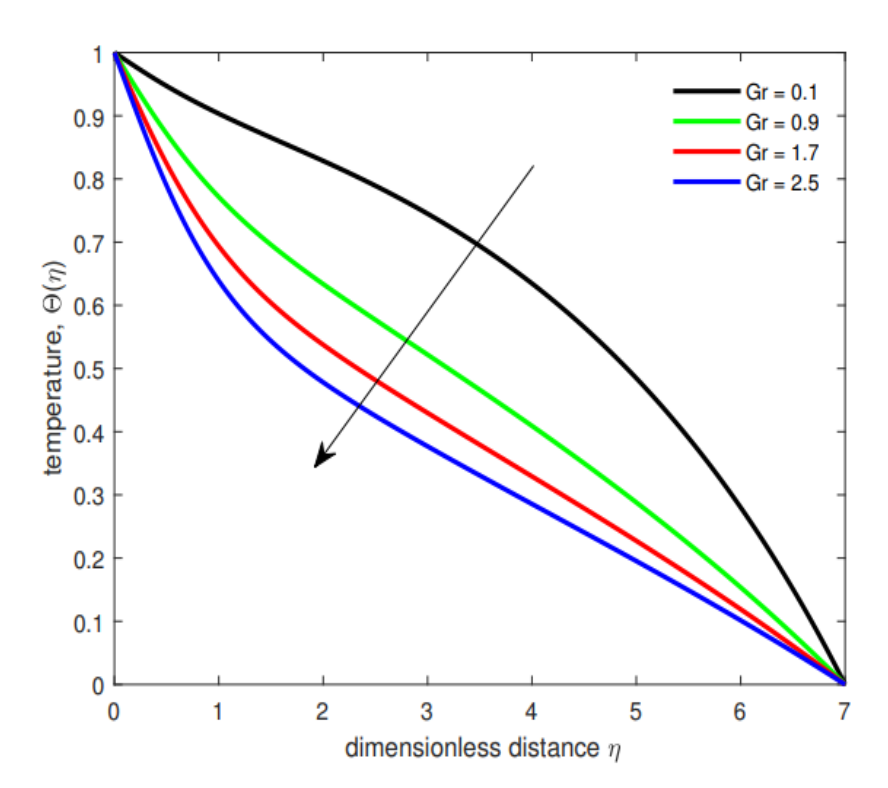
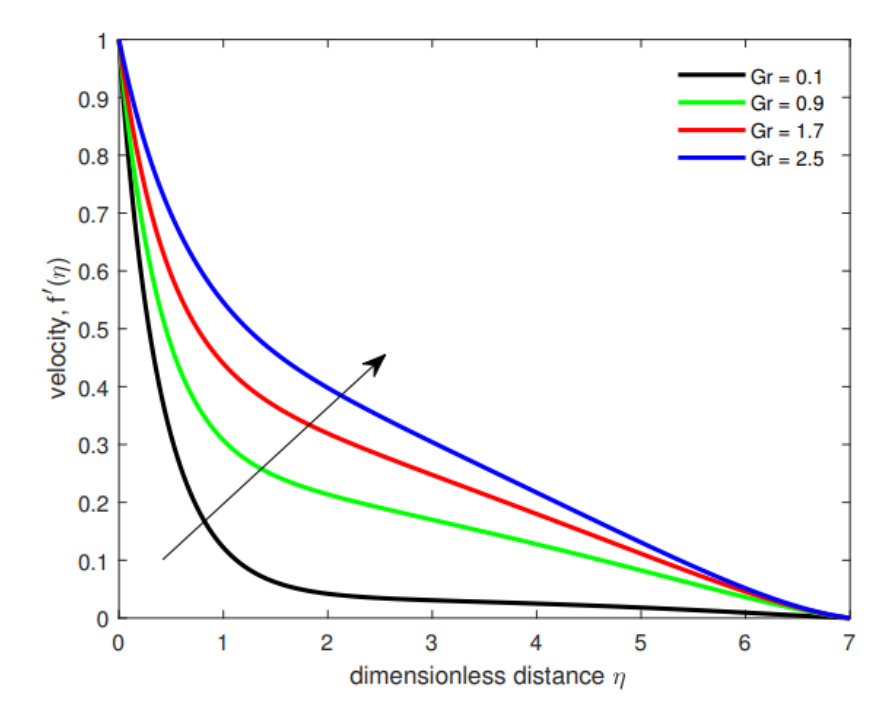


Figure 4.2: Effects of Velocity to Grashof number



## **Effect of Magnetic field**

A magnetised hybrid nanofluid flow experiences an opposing force called Lorenz force. This implies that Lorenz force becomes stronger as magnetism increases and therefore, the flow experiences more opposition. In this study, the magnitude of magnetism is obtained as

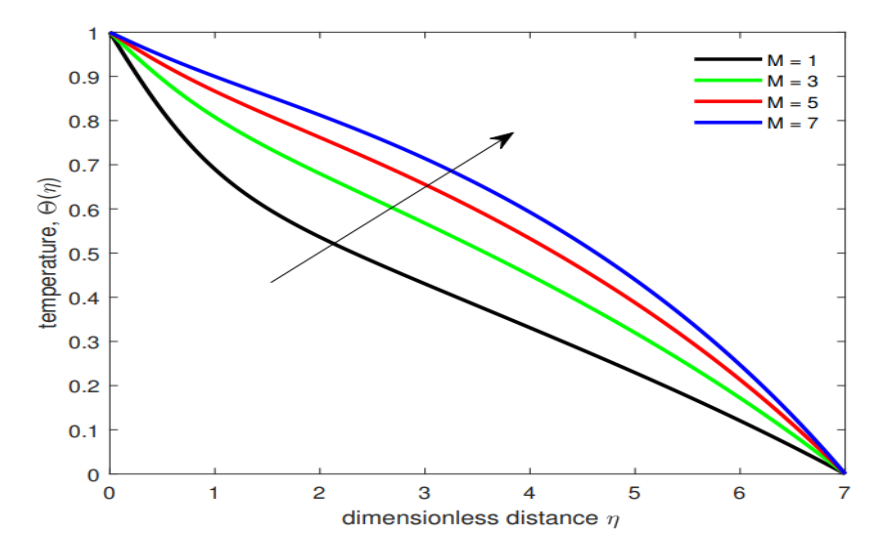
$$M = \frac{\sigma_f B^2}{a\rho_f}.$$

We increase M, consequently increasing Lorenz force, and study the response of temperature and velocity to increasing magnetism. Figures (4.3) and (4.4) display the behaviours. The stronger the magnetism, the higher



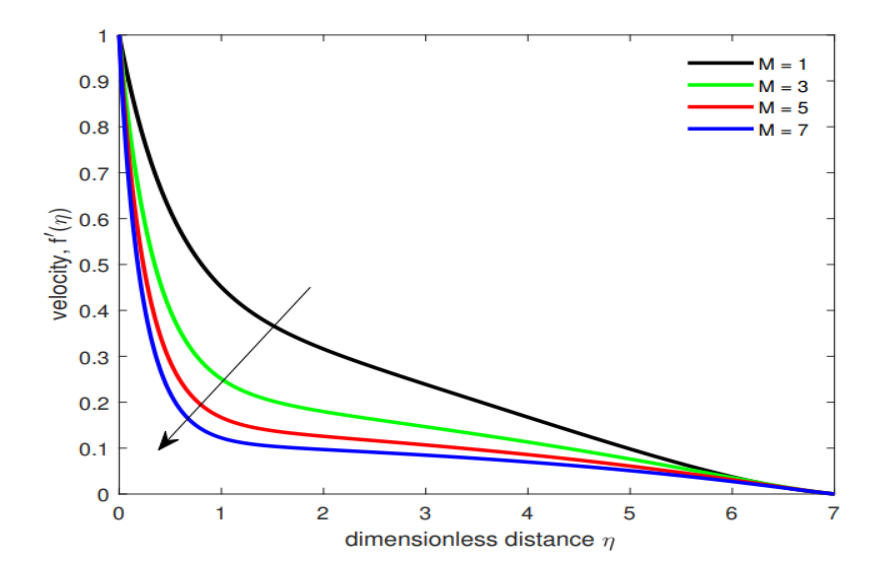
the temperature becomes but the lower the velocity. Fluid motion get impeded by the Lorenz force and thereby slow down the fluid particles, causing a reduction in velocity. The drag in the flow produce thermal energy which increases the temperature if the flow, hence an increase in flow temperature.

**Figure 4.3:** Effects of Temperature to Magnetism M on Temperature Profile  $\Theta(\eta)$ 



Higher magnetic parameters induce Joule heating through electrical resistance, elevating fluid temperature. Electromagnetic work dissipates as thermal energy, increasing Θ throughout. Arrows indicate temperature enhancement with stronger fields.

**Figure 4.4:** Effects of Temperature to Magnetism M on Velocity Profile  $f(\eta)$ 



Increasing M strengthens Lorentz force, opposing fluid motion and retarding momentum diffusion. This creates steeper velocity gradients near the wall and thinner momentum boundary layers, as arrows indicate.

#### **Effect of Volume Fraction**

The volume fractions for the nanoparticles are  $\phi_1$  and  $\phi_2$ , where 1 represents alumina (Al<sub>2</sub>O<sub>3</sub>) nanoparticles and 2 represents copper (Cu) nanoparticle. In this study, we have considered only the case where the two volume fractions are equal  $\phi_1 = \phi_2$ . Figure (4.5) shows the behaviour of the temperature of flow as  $\phi_1$  and  $\phi_2$  increase. The temperature increases as  $\phi_1$  and  $\phi_2$  get bigger. Increasing  $\phi_1$  and  $\phi_2$  increases the surface area of the solid particles and thereby allowing quick exchange of heat energy. This is responsible for the rise in temperature as  $\phi_1$  and  $\phi_2$  increase. However, figure (4.6) shows that velocity decreases with increasing  $\phi_1$  and  $\phi_2$ . Due to the

increase in  $\phi_1$  and  $\phi_2$ , nanoparticles agglomeration tends to cause a retardation in the flow and thereby reducing velocity as  $\phi_1$  and  $\phi_2$  gets larger.

**Figure 4.5:** Effects of Temperature to Volume fractions

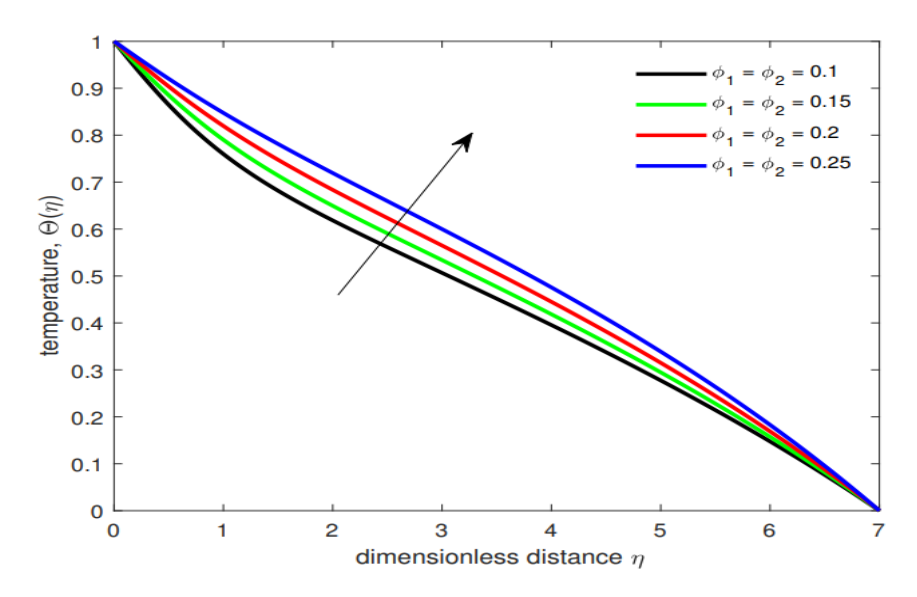
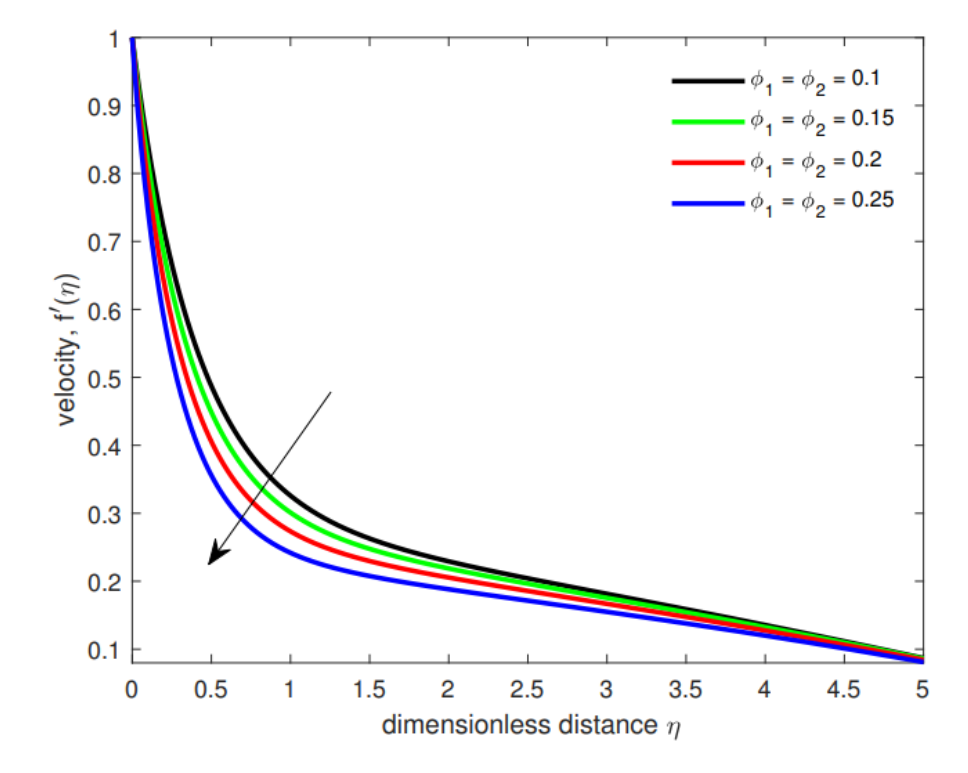


Figure 4.6: Effects of Velocity to Volume fractions



## CONCLUSION AND RECOMMENDATION

## Conclusion

This study considers the flow of fluid obtained by releasing two nanoparticles of different solid materials in the molten polyethylene. The flow is represented in mathematical form as a coupled PDE with some initialboundary condition, which is reformulated as a coupled ODEs by the use of similarity transformation. We employed the shooting technique to find an analogous the initial value problem to the initial-boundary condition problem. By varying a parameter while keeping other parameter fixed, the flow is simulated and the





## following results were obtained;

- Decrease in temperature and increase in velocity with Grashof number: As the Grashof number increases, indicating stronger buoyancy forces relative to viscous forces, the temperature decreases. This is because the fluid experiences less resistance from buoyancy, allowing it to flow more freely and increase in velocity.
- Magnetism raises temperature but lowers velocity: The introduction of magnetism increases the fluid temperature due to heat generation from magnetic nanoparticles. However, it also decreases fluid velocity, possibly due to altered flow patterns or increased frictional forces.
- Temperature increases but velocity decreases as volume fraction increases: Higher nanoparticle
  concentration leads to increased fluid temperature due to enhanced thermal conductivity or heat
  generation. However, the fluid velocity decreases as nanoparticles impede flow, causing greater
  resistance.

## **Industrial Applications**

These findings directly inform:

- **Heat exchanger optimization:** Tailoring nanoparticle concentration and magnetic fields maximizes heat transfer while minimizing pressure drop
- **Polymer extrusion control:** Adjusting thermal and flow parameters improves product uniformity and reduces defects
- Thermal management systems: Hybrid nanofluids offer superior cooling performance for electronics and automotive applications
- Magnetorheological processing: Magnetic field control enables real-time adjustment of flow and thermal characteristics

#### Recommendation

Based on the findings of this study, the following are recommended:

- 1. There is a crucial need for experimental validation of the simulation results. Conducting rigorous experiments would not only validate the accuracy of the model but also provide a real-world context for understanding the observed phenomena. By comparing simulation results with experimental data, researchers can gain confidence in the predictive capabilities of the model and refine it further.
- 2. Exploring the effects of varying nanoparticle properties, such as size, shape, and surface characteristics, could yield valuable insights. Understanding how these factors influence fluid behaviour and thermal dynamics could lead to the development of optimized nanoparticle designs for specific applications. This avenue of research has the potential to unlock new possibilities in areas such as heat transfer enhancement and nanofluid-based technologies.
- 3. In addition to nanoparticle properties, investigating the impact of external factors on the system is essential. Factors such as pressure variations, different fluid compositions, or external fields could significantly influence fluid flow and temperature distribution. Exploring these factors could not only expand the scope of potential applications but also enhance our understanding of the system's robustness and adaptability.

## REFERENCES

- 1. Ahmed, F., Reza-E-Rabbi, S., Ali, M. Y., Ali, L. E., Islam, A., Rahman, M. A., ... & Ahmmed, S. F. (2024). Numerical modeling of a MHD non-linear radiative Maxwell nano fluid with activation energy. Heliyon, 10(2).
- 2. Alfvén, H. (1942). Existence of Electromagnetic-Hydrodynamic Waves. Nature, 150(3805):405–406.
- 3. Ali, A., Kanwal, T., Awais, M., Shah, Z., Kumam, P., and Thounthong, P. (2021). Impact of thermal





radiation and non-uniform heat flux on MHD hybrid nanofluid along a stretching cylinder. Scientific

- Reports, 11(1).

  4. Ali, B., Ahammad, N. A., Awan, A. U., Oke, A. S., Tag-ElDin, E. M., Shah, F. A., & Majeed, S. (2022).
- 4. Ali, B., Ahammad, N. A., Awan, A. U., Oke, A. S., Tag-ElDin, E. M., Shah, F. A., & Majeed, S. (2022). The dynamics of water-based nanofluid subject to the nanoparticle's radius with a significant magnetic field: The case of rotating micropolar fluid. Sustainability, 14(17), 10474.
- 5. Allehiany, F. M., Bilal, M., Alfwzan, W. F., Ali, A., and Eldin, S. M. (2023). Numerical solution for the electrically conducting hybrid nanofluid flow between two parallel rotating surfaces subject to thermal radiation. AIP Advances, 13(7).
- 6. Algehyne, E. A., Alamrani, F. M., Khan, A., Khan, K. A., Lone, S. A., & Saeed, A. (2024). On thermal distribution of MHD mixed convective flow of a Casson hybrid nanofluid over an exponentially stretching surface with impact of chemical reaction and ohmic heating. Colloid and Polymer Science, 302(4), 503-516.
- 7. Asghar, A., Lund, L. A., Shah, Z., Vrinceanu, N., Deebani, W., and Shutaywi, M. (2022). Effect of thermal radiation on three-dimensional magnetized rotating flow of a hybrid nanofluid. Nanomaterials, 12(9):1566.
- 8. Choi, U. S. and Eastman, J. (1995). Enhancing Thermal Conductivity of Fluids with Nanoparticles. ASME International Mechanical Congress and Exposition, San Francisco, (12–17).
- 9. Farooq, U., Lu, D., Munir, S., Ramzan, M., Suleman, M., and Hussain, S. (2019). MHD flow of maxwell fluid with nanomaterials due to an exponentially stretching surface. Scientific Reports, 9(1).
- 10. Fatunmbi, E. O., Badru, J. O., & Oke, A. S. (2020). Magneto-Reactive Jeffrey Nanofluid Flow over a Stretching Sheet with Activation Energy, Nonlinear Thermal Radiation and Entropy Analysis.
- 11. Govindarajulu, K., & Subramanyam Reddy, A. (2022). Magnetohydrodynamic pulsatile flow of third grade hybrid nanofluid in a porous channel with Ohmic heating and thermal radiation effects. Physics of Fluids, 34(1).
- 12. Hady, F. M., Ibrahim, F. S., Abdel-Gaied, S. M., and Eid, M. R. (2012). Radiation effect on viscous flow of a nanofluid and heat transfer over a nonlinearly stretching sheet. Nanoscale Research Letters, 7(1).
- 13. Jaafar, A., Waini, I., Jamaludin, A., Nazaar, R., and Pop, I. (2022). Mhd flow and heat transfer of a hybrid nanofluid past a nonlinear surface stretching/shrinking with effects of thermal radiation and suction. Chinese Journal of Physics, 79:13–27.
- 14. Jayaprakash, J., Govindan, V., Santra, S. S., Askar, S. S., Foul, A., Nandi, S., & Hussain, S. M. (2024). Thermal radiation, Soret and Dufour effects on MHD mixed convective Maxwell hybrid nanofluid flow under porous medium: a numerical study. International Journal of Numerical Methods for Heat & Fluid Flow, 34(10), 3924-3952.
- 15. Khan, N., Ali, F., Ahmad, Z., Murtaza, S., Ganie, A. H., Khan, I., & Eldin, S. M. (2023). A time fractional model of a Maxwell nanofluid through a channel flow with applications in grease. Scientific Reports, 13(1), 4428.
- 16. Kigio, J. K., Mutuku, W. N., & Oke, A. S. Analysis of volume fraction and convective heat transfer on MHD Casson nanofluid over a vertical plate, Fluid Mechanics, 7 (2021), 1–8.
- 17. Maxwell, J. C. (1873). A Treatise on Electricity and Magnetism. Nature, 7:478–480.
- 18. Rajesh, V., Srilatha, M., and Chamkha, A. J. (2020). Hydromagnetic effects on hybrid nanofluid (cualuminium-water) flow with convective heat transfer due to a stretching sheet. Journal of Nanofluids, 9(4):293–301.
- 19. Sakiadis, B. C. (1961). Boundary-layer behavior on continuous solid surfaces: I. boundary-layer equations for two-dimensional and axisymmetric flow. AIChE Journal, 7(1):26–28.
- 20. SAMUEL, O. A. (2022). Coriolis Effects on Air, Nanofluid and Casson Fluid Flow Over a Surface with Nonuniform Thickness. PhD diss., KENYATTA UNIVERSITY
- 21. Suresh, S., Venkitaraj, K., Selvakumar, P., and Chandrasekar, M. (2011). Synthesis of al2o3–cu/water hybrid nanofluids using two step method and its thermo physical properties. Multidisciplinary Digital, 388(1-3):41–48.
- 22. Vijay, N., & Sharma, K. (2023). Dynamics of stagnation point flow of Maxwell nanofluid with combined heat and mass transfer effects: A numerical investigation. International Communications in



- Heat and Mass Transfer, 141, 106545.
- 23. Wang, F., Jamshed, W., Ibrahim, R. W., Abdalla, N. S. E., Abd-Elmonem, A., & Hussain, S. M. (2023). Solar radiative and chemical reactive influences on electromagnetic Maxwell nanofluid flow in Buongiorno model. Journal of Magnetism and Magnetic Materials, 576, 170748.
- 24. Zainal, N. A., Nazar, R., Naganthran, K., and Pop, I. (2022). The impact of thermal radiation on maxwell hybrid nanofluids in the stagnation region. Multidisciplinary Digital Publishing Institute.

#### The Matlab Code

```
clc; clear all; format compact
global We Gr M Pr R Q phi mu_f phi kappa sigma rho cp
mu f = 18.376; We = 0.1; Gr = 1; M = 2; Pr = 7; Q = 0.21; R = 0.1;
phi = [0.1, 0.1]; tspan=linspace(0,7,500); x_initial = zeros(1,5); i=1;
%nanoparticles are Al2O3 and Cu
%base fluid is molten polyethylene
kappa = [40, 400, 0.253]; sigma = [6.3e7, 4.25e7, 10.7e-5];
rho = [3970, 8933, 1115]; cp = [765, 385, 2430];
Legend_Entries = []; txt_var = "phi"; Line_Style = ["k-", "g-", "r-", "b-"];
for Val = [0.1, 0.15, 0.2, 0.25]
  phi = [Val, Val];
  solinit=bvpinit(tspan,x_initial);
  sol = bvp4c(@Fluid,@Bc,solinit);
  t = sol.x; s = sol.y;
  %Legend_Entries = [Legend_Entries,strcat(txt_var," = ", num2str(Val))];
  Legend Entries = [Legend Entries, strcat("\phi 1 = \phi 2 = ", num2str(Val))];
  txt = Line_Style(i);
  if i \sim = 4
    figure(2), plot(t,s(2,:),txt,'LineWidth',2)
    hold on
    figure(4), plot(t,s(4,:),txt,'LineWidth',2)
    hold on
  elseif i == 4
```



```
figure(2), plot(t,s(2,:),txt,'LineWidth',2)
    xlabel(" dimensionless distance \eta")
    ylabel("velocity, f^\prime(\eta)")
    legend(Legend_Entries); legend('boxoff')
    txt_vel = strcat(txt_var,"_velocity");
    saveas(gcf,txt_vel,'fig')
    figure(4), plot(t,s(4,:),txt,'LineWidth',2)
    xlabel(" dimensionless distance \eta")
    ylabel("temperature, \Theta(\eta)")
    legend(Legend_Entries); legend('boxoff')
    txt_temp = strcat(txt_var,"_temperature");
    saveas(gcf,txt_temp,'fig')
end
i=i+1;
end
function res = Fluid(eta,x)
global We Gr M Pr R Q phi mu_f phi kappa sigma rho cp
  f = x(1); f_p = x(2); f_p = x(3); theta = x(4); theta_p = x(5);
  PHI = sum(phi);
  A1_num = 2*(1-PHI)*PHI*kappa(3) + (1 + 2*PHI)*sum(phi.*kappa(1:2));
  A1_den = (2+PHI)*PHI*kappa(3) + (1 - PHI)*sum(phi.*kappa(1:2));
  A1 = A1_num/A1_den;
  A2_num = 2*(1-PHI)*PHI*sigma(3) + (1 + 2*PHI)*sum(phi.*sigma(1:2));
  A2_den = ((2+PHI)*PHI*sigma(3) + (1 - PHI)*sum(phi.*sigma(1:2)));
  A2 = A1_num/A1_den;
   A2 = (1-PHI + sum(phi.*sigma(1:2))/sigma(3));
  A3 = 1 - PHI + sum(phi.*rho(1:2).*cp(1:2))/(rho(3)*cp(3));
  A4 = 1 - PHI + sum(phi.*rho(1:2))/rho(3);
```

```
A5 = 0.904*exp(0.148*PHI); \\ dx1 = x(2); dx2 = x(3); \\ dx3 = (f_p^2 - f^*f_pp - Gr^*theta + (A2/A4)^*M^*f_p)/((A5/A4) + We^*f_pp); \\ dx4 = x(5); \\ dx5 = (-f^*theta_p + Q^*(theta - 1)/A3)/(A1/(A3*Pr) + (4*R/3)); \\ res = [dx1, dx2, dx3, dx4, dx5]; \\ end \\ function res = Bc(y0,yinf) \\ global We Gr M Pr R Q phi mu_f phi kappa sigma rho cp \\ res = [y0(1) \\ y0(2)-1 \\ y0(4)-1 \\ yinf(2) \\ yinf(4)]; \\ end
```